Study of $J/\psi \to \mu^+\mu^-$ Decays Using the H1 Detector at HERA

Craig Wiglesworth
September 12, 2005

Abstract

The study of the effects of different track selections in analyses of muon pairs originating from J/ψ decays, in which one of these muon is detected in the central tracking detector (CTD) and the other is detected in the forward tracking detector (FTD), is investigated. A set of track selections have subsequently been chosen with aim of maximising both the efficiency of H1's forward tracking detector and the resolution of the J/ψ signature peak. The study is made for both vertex fitted and non-vertex fitted muon tracks.

1 Introduction

The HERA facility located at DESY in Hamburg is unique in that it is the only electron-positron collider in the world. Since 1992 the collision experiments H1 and ZEUS have recorded over 200pb^{-1} of data, at a centre of mass energy of up to 319 GeV (note that natural units are used throughout this report). Through analyses of these data a variety of physical phenomena, both particle physics within and beyond the Standard Model have since been studied. One such study has been that of J/ψ particle production in high energy collisions, and their subsequent decay into lepton pairs.

The investigation presented in this report describes how a J/ψ analysis package is used to analyse such decays, and in this particular case those decays that result in the formation of muon pairs. The aim of the investigation is to use this J/ψ analysis package in order to determine a set of muon track selections that will optimise the performance of H1's forward tracking detector (FTD), with respect to its efficiency and invariant mass peak resolution.

The report is organised as follows. Chapter 2 provides an introduction to HERA, followed by a thorough description of the H1 detector in chapter 3. The J/ψ particle is introduced in chapter 4 and a brief discussion of the H1OO Analysis Framework is presented in chapter 5. Chapter 6 describes the main topics of discussion and areas of particular interest, followed by the results of the investigation which are found in chapter 7. Chapter 8 concludes the report with a brief summary of the investigation and finally, chapter 9 is dedicated to all those people without whom I would not have been able to perform this invesigation.

2 HERA

The HERA (Hadron Electron Ring Accelerator) storage ring (see figure 1), workplace of 950 particle physicists from around the world, is situated 7 stories beneath the ground in the German city of Hamburg and since its 8 year preparation phase (1984 - 1992) its has been the only electron proton collider in the world. The ring itself is an almost circular structure with a circumference of 6.3km, the majority of which lies outside the DESY site and actually consists of two layered concentric evacuated beam pipes, the top of which is a proton storage ring and the bottom an electron storage ring. (Here the name electron will be used generically to describe both electrons and positrons, unless otherwise stated). HERA accelerates and collides positrons with protons, although in 1998 there was a period of time in which electrons were used rather than positrons, during which the integrated luminosity per year delivered by HERA was steadily increased. HERA is also capable of accelerating and colliding deuterium nuclei with electrons, although these interactions are have rarely been a hot topic for investigation. The accelerating mechanisms are slightly different for the electron and the proton beams due to their differing properties. The magnetic fields required to accelerate electrons can be produced by normal conducting magnets operating at room temperature, whereas 4.7T superconducting magnets operating at 4.4K are required to curve the path of the high momentum proton beam. The high energy electron and proton beams lead to currents in the beam pipes typically in the region of 30mA and 80mA respectively. These large beam currents are not just a consequence of requiring high energy collisions, they are indeed a requirement in itself as the electron positron

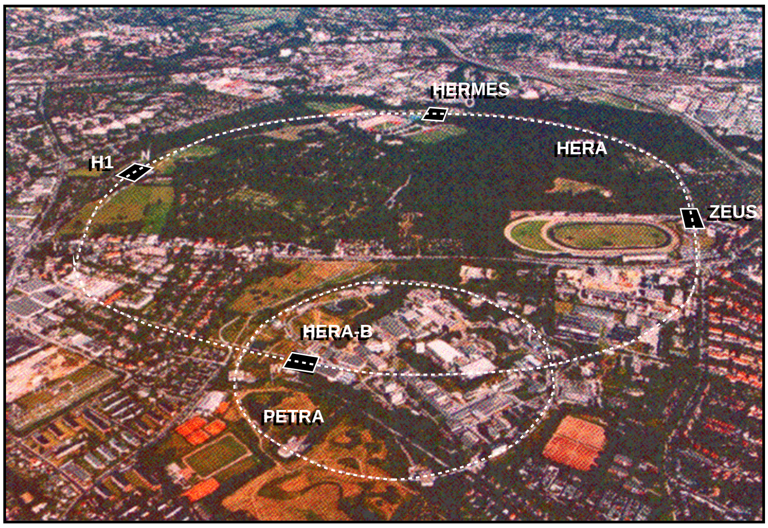

Figure 1: An aerial view of the HERA and PETRA accelerators at DESY.

interaction cross section is small. The eariler storage rings on the DESY site that were once the basis of DESY's particle interaction studies before the construction of HERA (such as LINAC, DESY II, DESY III, PETRA), are now operated as pre-accelerators for the electrons and protons which are evetually passed into the HERA ring at energies of approximatley 12 GeV and 40 GeV respectively. Within the HERA ring the electrons and protons are accelerated in their respective storage rings in approximately 220 bunches, each containing of order 10^{11} particles. The density of these particle bunches follows a gaussian distribution with a width of 1cm (11cm) for electrons (protons) and follows in the logitudinal direction of the beam.

Each of these particle bunches is separated by 96 ns, and they are continuously accelerated until the electron and proton energies reach their respective target energies of 27.6 GeV and 920 GeV, corresponding to a centre of mass energy of $\sqrt{319}$ GeV. (It is interesting to note at this point that prior to a HERA upgrade in 1998, the electron and proton beam energies were 27.6 GeV and 820 GeV respectively, resulting in a centre of mass energy of $\sqrt{300}$ GeV). Prior to HERA it was not possible to achieve such centre of mass energies; the current value is indeed a factor of ten times greater than the values attainable in earlier accelerator/storage machines in which electrons were incident on fixed target protons, thus permitting a more intrusive analysis of particle interactions. The values of the beam energies represent limits set by the effect of synchrotron radiation emission from the electron and the attainable magnetic field strength required to accelerate the protons. It is worth noting that since the emission of synchrotron radiation scales as $\frac{1}{m^4}$, the comparatively large mass of the proton results in negligible energy losses through synchrotron emission. As the particle bunches are accelerated around the beam pipe, the proton bunches become compressed and their resulting complicated logitudinal structure often leads to particle migrations in which small "satellite" bunches are formed. These are accelerated in common with, but separated from, the main bunch by up to 8ns, and lead to background due to interactions with electrons from the electron beam in regions of the detector other than the nominal interaction region. Of the 220 electron and proton bunches, only approximately 176 of these will interact. The remaining bunches, known as pilot bunches, do not collide with bunches from the opposing beam, but are rather used to inhibit interactions with either the beam pipe walls or with the residual gases that exist in the beam pipe, providing a means of studying the origin and rates of background signals.

The counter rotating beams are brought together to collide at specific points on the HERA ring. There are two detectors that have been operational since 1992, H1 and ZEUS, which are situated in the northenmost and southernmost parts of the ring respectively. Each of these detectors utilises different detection techniques to measure the energy and track the positions of the particles and jets created in the high energy electron proton collisions. There are two other ”fixed target” detectors; HERMES in the far East and HERA-B in the far West, each of which investigates the interactions between either one of HERA’s accelerated beams and specific fixed targets. The HERA-B detector became operational in 2000 with the intention of searching for violations of charge parity (CP) conservation in the decay of the heavy quarks present in B and B-bar mesons, ($B^0 \rightarrow J/\psi$ + Ks^0). These experiments were based on the interactions of those protons constituting the halo of HERA’s high energy proton beam, incident on a specified fixed target. HERA-B stopped taking data in 2003. Similarly, the HERMES detector makes use of a phenomenon known as the Sokolov Ternov effect in which the propagating electron beam becomes natually transversely polarised over a period of time due to its synchrotron emissions. By employing spin rotators around the beam pipe to transform the transversley polarised beam into a longituduinally polarised beam and vice versa, HERA’s longitudinally polarised positron beam is used to investigate the spin structure of the nucleon by colliding the beam with a stationary polarised Hydrogen, Deuterium or Helium gas target. In 2000-2002 HERA underwent an extensive remodelling to enhance its performace capabilities, and became operational again in 2001. The pre-2001 operational period is known as HERA ”phase I”, and similarly, since the 2001 upgrade HERA has been operating in ”phase II”. The impending introduction of the Large Hadron Collider (LHC) [1] at CERN seemed to spell the end for HERA, although the current plan is continue operations until decomissioning in 2007. Until then HERA will continue to provide the necessary high energy requirements of a promising physics program that includes studies of proton structure, photon structure, perturbative QCD, non-perturbative QCD, diffraction and maybe hitherto unseen physical processes beyond the Standard Model.

3 The H1 Detector

The H1 detector [2] is situated at the northernmost point of the HERA ring, specifically detecting and measuring the energetic products of the high energy collisions that are produced when the detector’s focussing magnets brings the electron and proton beams together. The current H1 experiment is an international collaboration of about 400 physicists from 40 institutes in 15 countries, in which the internal structure of the proton is being probed with an unprecedented accuracy, whilst still retaining the capabilities to detect any as of yet unobserved particles. The experiment is the only one of its kind in the world and aims to shed some new light on the particles and fundamental forces that constitute the world in which we live. The detector itself has an approximate volume of 12m x 10m x 15m and weighs somewhere in the region of 2800 tonnes. Its structual features are highly assymetric, reflecting the assymetric beam energies.

As expected, the trajectories of many of the final state particles are (in the lab frame) boosted in the direction of the incident proton beam and to achieve refined high resolution measurements of these particles, the number and volume of detector components with high sensitivity and granularity are located in this region. Another striking structural feature of the detector is that there is almost full solid angle (4π) coverage around the interaction point, with the only limitation originating from the beam pipe itself. This is of particularly importance as the electron proton interactions often result in final state neutrinos and since these neutrinos cannot be identified directly, they can only be inferred via an imbalance of the net transverse momentum of all the other final state particles. Each of these structural features are implemented in order to maximise the attainable efficiency in obtaining as much information from the electron proton collision as possible.

In describing the schematics of the detector (see figure 2), the interaction point is defined as the origin of a right handed Cartesian co-ordinate system in which the x axis is directed towards the centre of the HERA ring, the y axis is vertically upwards and the z axis is the direction of the incident proton beam. Similarly in the corresponding spherical co-ordinate system the polar angle (θ) is defined as zero with respect to the proton beam direction and the azimuthal angle (ϕ = arctan (y/x)) is positive in the positive y direction. It should also be mentioned that the positive z axis direction is referred to as the forward direction and consequently the negative z axis direction is defined as the backward direction.

The H1 detector employs two main methods of particle identification each of which is based on two different detection techniques: Tracking and calorimetry. The tracking system is located in the immediate vicinity of the interaction point in a cylindrical arrangement that complements the structure of the beam pipe. The tracking detectors are situated within a 1.15T magnetic field, provided by a superconducting solenoid of diameter and length 5.8m which is cooled to 4°C by liquid helium from DESY's central refrigerator plant. The presence of the magnetic field allows the identification of the charge and momenta of the intersecting particles via their radius of curvature. Surrounding the superconducting coil is a 2000 tonne mass of iron which not only provides the return yoke but also houses many detectors, each with the aim of recording any residual particles that leak out through the back of the inner detector regions and any penetrating particles such as muons that can completely traverse the inner components. The calorimeters are situated immediately outside the tracking detectors, but still within the layer of instrumented iron. Their main role is to absorb the energy of the final state particles by inducing continuous cascades of particle showers, until the energy of the particle incident on the calorimeter is completely absorbed by the calorimeter components. As in the case of the tracking detectors, the calorimeter components have a high layer of granularity to provide appropriate precision and energy resolution. A further detector is situated outside the iron return yoke in the forward direction to detect muons penetrating the H1 detector at low polar angles. The whole H1 detector as described so far is then surrounded by concrete shielding, and in order to ensure that the magnetic field originating from the solenoid doesn't interefere with HERA's particle beam trajectories, a superconducting compensation coil opposing the direction of the initial magnetic field is also implemented. Within each of these detector systems there is yet more segregation into individual sub-detectors and components. These are described in more detail below.

The tracking system (see figure 3) is segregated into three specific sub-detector regions, the central tracking detector (CTD), the forward tracking detector (FTD) and the backward proportional chamber / backward drift chamber (BPC/BDC). Within the central tracking detector is the central silicon tracker (CST) surrounding the nominal interaction point which provides accurate charged particle tracking and an indication of the primary interaction vertex position and

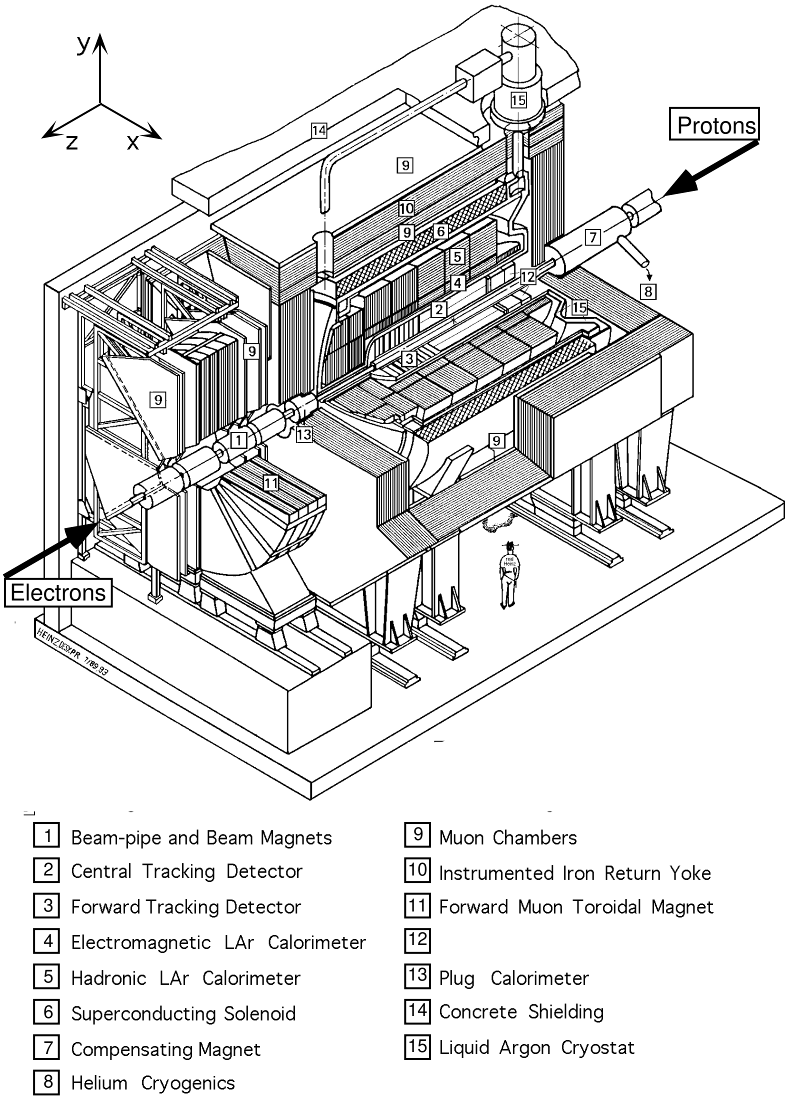

Figure 2: A schematic diagram of the H1 detector.

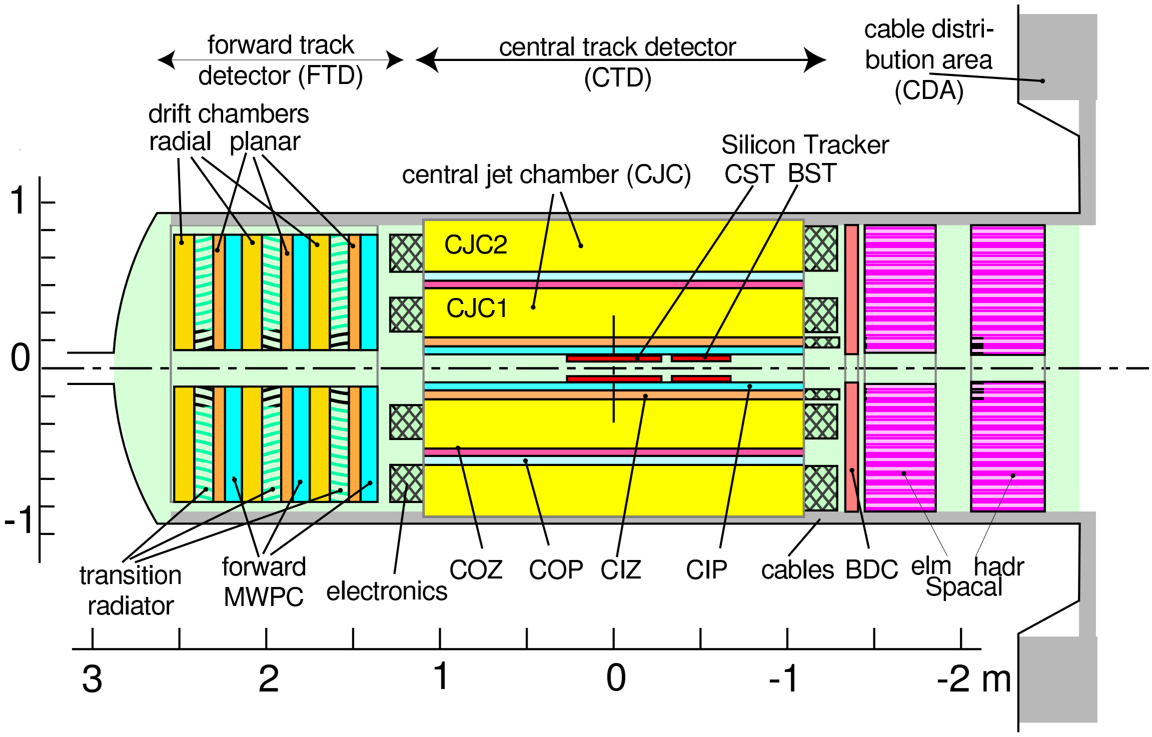

Figure 3: Tracking detectors in the H1 detector.

backward silicon tracker (BST) which detects the position of secondary vetices and the angles at which the incident beam electrons are scattered into the backward regions.

The calorimetry system is a made of four separate sub-detectors (see figure 2). Primarily, there is an arrangement of steel and lead plates which are submerged in $-183°$C cryostat cooled, liquid Argon. This liquid argon (LAr) calorimeter operates in the forward and central regions of the H1 structure (in the range $4° \leq \theta \leq 153°$), and can be 5 to 8 interaction lengths deep depending upon the polar angle at which the particle transverses the calorimeter. Its purpose is to measure the electromagnetic and hadronic showers that are created by the incident high energy particles on the lead and steel plates respectively. Such calorimeter systems allow the products of the proton "fragmentation" to be detected, upon its collision with the electron. This fragmentation of the proton leads to the emission of quarks and gluons which are forbidden to appear free in nature, and thus result in jets of particles sprayed from the interaction point. It is the absorption of the energy of these jet particles that results in the electrical signals that provide a recordable measure of the energy and direction of the jets.

The spaghetti calorimeter (SpaCal) operates exclusively in the backward regions ($153° \leq \theta \leq 177.5°$), and specifically detects the scattered electron, along with any other backward going hadronic particles. In order to maximise solid angle calorimeter coverage around the interaction point, a Plug calorimeter is situated around the beam pipe to "plug" the gap between the LAr and the beam pipe and also to measure hadronic activity in the low polar angle range ($0.75° \leq \theta \leq 3.4°$).

Finally, as mentioned earlier there is a collection of tail catcher calorimeters situated in the return yoke of the solenoid which consist of a large array of plastic streamer tubes each with a single signal wire mounted down the centre. Tracking of highly penetrating final state muons, which traverse the inner tracking and calorimetry devices, is possible by reconstruction of the signal patterns recorded in these streamer tubes. The high penetrative nature of the muon is therefore the means through which they are distinguished from other final state particles. Conversely, final state muons in the forward region ($3^\circ \leq \theta \leq 17^\circ$) are detected by a separate forward muon detector (FMD) which contains an iron toroid to again identify the charge and momenta of the particles through thier radius of curvature. The FMD consists of 12 layers of drift chambers, 6 layers either side of the toroid magnet.

Outside the detector, in the forward regions of the beam pipe there are also forward proton spectrometers (FPS) and a forward neutron calorimeter (FNC) each of which was introduced with the aim of investigating interactions containing a leading baryon.

Due to the multi-purpose nature of the H1 detector it is possible to study a variety of different experimental phenomena. Such topics of interest include cross section measurements of both charged and neutral current events, production of heavy quarks, measurements of QCD processes, diffraction, and as of yet unobserved physics such as quark substructure, leptoquarks and magnetic monopoles that would currently be considered out of place in the Standard Model. The huge number of electron proton events that occur each second, subsequently leads to a mass of information collected from all the detector systems throughout the H1 structure. Unfortunately the rate at which this data can be processed is limited, and because the rate of interactions is so high it is not possible to record the information from every single collision. Consequently, various trigger systems are employed that filter out certain interaction data, such that only data with specific (user-defined) ”interesting” features are stored. The information which is readout from these interactions of interest is stored on magnetic tape catridges at the DESY central mainframe computer for subsequent analysis.

4 Introduction To The J/ψ Particle

The J/ψ particle is an uncharged spin zero meson constructed from a bound state of a charm quark anti-quark pair, each of which move with small velocities in the rest frame of the J/ψ. This bound state is known as charmonium and is analgous to the structure of positronium. The double name originates from the fact that the particle was discovered almost simultaneously by two independent research groups investigating different high energy particle collisions. Burton Richter led a team of physicists at the Stanford Linear Accelerator Centre (California) in the study of high energy electron positron collisions (annihilations), whilst another team led by Samuel Ting studied the interaction of high energy protons on a stationary Beryllium target at the Brookhaven National Laboratory (New York). Although these investigations initially followed different paths, their analyses were both found to share a striking feature. After calculating the invariant mass of each respective electron and muon pair, each of the groups observed a resonance at 3.096 GeV/c^2 and immediately concluded that this was the signature of a previously unobserved particle. The particle was subsequently named the ψ particle by Richter and the J particle by Ting. Due to the simultaneous nature of the two discoveries, the scientific community suggested that it would be unjust to credit the particle with just one name and so the particle became known as the J/ψ particle.

The particle was also observed to have an unusually narrow resonance peak, which via Heisenberg's Uncertainty principle, corresponds to a relatively long lifetime (0.8×10^{-20}) seconds. It was highly unexpected that such a particle could posess this property and it was the subsequent attempts to explain this phenomena that led to the discovery of the charm quark. Indeed, the lightest meson which was known at the time was the D^0 meson (containing one charm quark), which had a mass of 1.865 GeV/c^2. Since the combined masses of a D^+ D^- pair exceeds the mass of the J/ψ particle, it is energetically impossible for the J/ψ to decay into lighter mesons as initially expected. Similarly, the colourless nature of the J/ψ means that decays via the strong interaction are almost completely forbidden; the only possible interaction involves the emission of three gluons of colour charges red, green and blue, a process which is *Zweig suppressed*.

Hadronic decays provide the greatest contribution to the total number of J/ψ decay channels, although the aforementioned suppressions of certain decay channels means that there is still a significant branching ratio for the electromagnetic decays. This is rather fortunate since the di-lepton decays of the J/ψ into electron or muon pairs, (each of which has a branching ratio of approximately 6%), provide a means of recreating a particularly clean J/ψ signature peak from the invariant mass of each lepton pair. Such a decay to muons is the subject of this report, and is described in section 6.

Since the discovery of the J/ψ particle, a detailed spectrum of all charmonium states (of which the J/ψ is the lowest mass state) has been produced. In this charmonium spectrum the radially excited, higher mass states of the J/ψ are known as ψ states since these higher mass particle were first observed by Richter and his team. For example the first excited state, which has a mass of 3683 MeV, is labelled the ψ(3686). Similarly, the first excited state that is permitted to decay into a pair of charmed D^0 mesons is the ψ (3770), which consequently displays a broader resonance that is more in keeping with typical hadronic decays. These broader resonances are more difficult to identify experimentally making the higher mass states less well measured.

J/ψ production, or more precisely heavy quark production is a useful tool that has been implemented by HERA to investigate different aspects of physics, in particular Quantum Chromo-Dynamics. When a charm anti-charm quark pair are created in an interaction, the two particles must be produced with relatively low momenta (in the quark anti-quark frame) in comparison to the mass of the particles. If this is the case then the two particles will form a bound charmonium state, otherwise the quarks will hadronise each forming a charmed meson. The production of these charmonium states and the charmed particles are known as hidden charm and open charm production methods, referring to whether the overall charm quantum number of the final state particles is 0 or 1. These charmonium states can be produced via both elastic and inelastic interactions using HERA's high energy electron and proton beams. For inelastic collisions there is a transfer of colour charge between the proton and the final charmonium state, and as a result the proton fragments into a variety of hadrons which, together with the decay products of the meson, go to make up the final state particles. Similarly, in elastic charmonium production via the diffractive process, the proton remains intact or at most dissociates into fragments with low transverse momenta (see figure 4). These elastic and inelastic processes can either be in the context of deep inelastic scattering or photoproduction, and each different process dominates in different kinematic phase space regions of HERA.

Prior to the discovery of the J/ψ particle there was a model in place in which the up, down and strange quarks were already known. One important feature of this model had been that

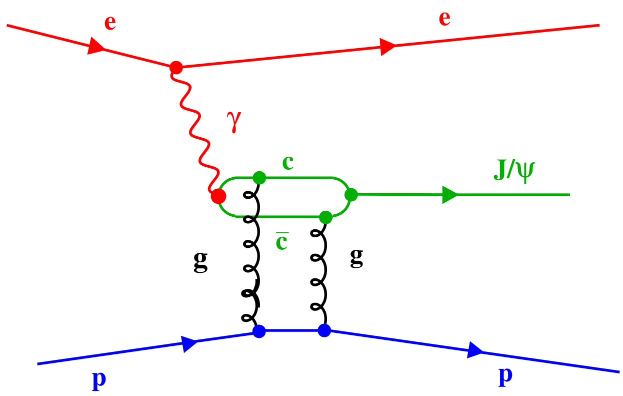

Figure 4: The mechanism of elastic J/ψ production in ep collisions at H1.

the different quark flavours should come in pairs, in which the up and down quarks constitute the first generation. It was therefore also expected that the strange quark would take its place in the second generation, but at the time a complementary second generation particle had not been observed. The discovery of the J/ψ and the subsequent discovery of the charm quark lead to massive and rapid developments in the field of particle physics; so much so that the period in which the discovery was made is often referred to as the November Revolution. The signature resonance peak of the J/ψ particle had in fact been seen some years earlier in an experiment led by Leon M. Lederman, although his inability to explain the peak's origin meant that he was never credited with discovering the J/ψ particle. In 1976 Richter and Ting were awarded the Nobel Prize. Even now, more than 25 years after its discovery, the J/ψ particle still figures predominantly in modern particle physics investigations, due to its clean experimental signature.

5 Introduction To The H1OO Analysis Framework

The Object Oriented framework [3] was introduced to provide an improved and combined data storage and analysis environment for H1. This centralised physics analysis software is structured within the ROOT [4] framework, which is an object oriented framework written in the C++ programming language. The framework offers a wide selection of tools that allow H1 analyses to be completed with high peformance and improved efficiency. Documentation [6] describing the purpose of each class, it's data members, member functions, source code, and the parent class from which each class is derived is also easily provided.

After the Production Output Tape (POT) which tops the data storage hierarchy, the H1OO framework (see figure 5) has 3 official data layers:

- The Object Data Storage (ODS) layer for the reconstruction output. This layer consists of reconstructed tracks, clusters and detector level information.
- The Micro Object Data Storage (μODS) layer for physics particles. This is the main analysis layer and contains particle candidates, along with identified and composed particles that are reconstructed by the ODS information.

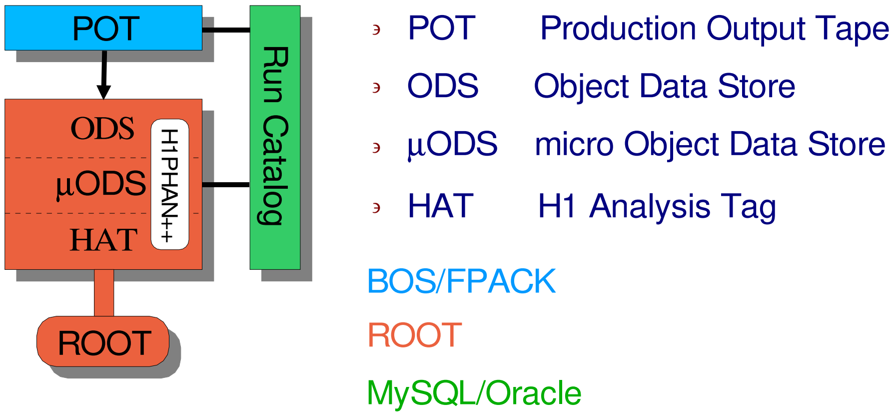

Figure 5: The data storage and analysis schemes of H1.

- The H1 Analysis Tag (HAT) layer for basic type quantities. This provides a consise summary of the characteristic features of the events and can be used to perform quick event selections.

Any combination of the ODS, μODS and HAT layers can be analysed using ROOT combined with the H1OO framework. A further, optional layer is the UserTree layer containing additional user information. Some information that is very specific to a particular analysis, which may not be present in the ODS, μODS or HAT, and is therefore stored separately in such UserTrees.

Although the above data storage layers are themselves stored in separate files, each layer is linked to one another by the H1Tree which is the user interface to all data in the h1oo framework. In object oriented programming independent modules are responsible for their own data, and must themselves be able to supply any and all information about the data they contain whilst maintaining integrity. In this way the data contained in the module or object can be decoupled from the complete system, significantly reducing the complexity of the problem at hand. Together with the applicability of OO programming principles such as abstraction, inheritance and encapsulation, these modules can be structured in such a manner as to create a highly effficient analysis framework. This is indeed the basis of the H1OO framework, which consists of a large construct of interacting classes from which an arbitrary number of objects can be constructed.

When a typical analysis is decomposed into consecutive layers or of simpler processes, the benefits of applying an OO framework become more evident. For example any H1 analysis scenario can be generalised by decomposing the analysis into a series of layers or levels, each of which provides a different contribution to the overall analysis, which is somewhat independent of the contributions from all the other levels. This is the aim of the H1Lt analysis code [5], which interfaces the H1OO project and is described below.

The first level (or `Analysis` level) is the stage at which the steering control and initialisation are defined. The use of steering allows the properties of a particular object to be altered without having to recompile any code. Within this level, the different `AnalysisChains`, the `BinGrids` and the `EventSelectors` are defined, and there can be any number of these objects. Each `AnalysisChain` stores the `HistManager` and `Measurements` objects and the actual behaviour of the chain is determined by its `EventLoop` member function, which defines the function of the `AnalysisChain` object for each event. It is often necessary to create multiple histograms in any particular analysis, and therefore the function of the `HistManagers` is to provide an interface for several individual histogram objects. The `EventSelection` objects also adhere to their own specific structure consisting of another 3 levels, namely the reconstructed level, the generator level and the Monte Carlo (MC) phase space level, together with the various `Cut` objects. The `Cuts` objects are stored in a list of cuts (`CutList`) which provides an interface for applying all cuts. The `EventSelector` consists of three of these `CutLists`, one for the reconstructed level properties of an `Event` for both data and simulation, one for the generator level properties of a simulated event and one for the purpose of selecting the generator level phase-space for a given simulation.

The next level is the `AnalysisChain` level, at which point the files containing the experimental data and MC are loaded such that one set of files corresponds to each previously defined `AnalysisChain` object. Generic, coherent access to the data is provided by the `H1Calculator` H1OO package. The `AnalysisChains` also interface the `BinGrid` and `EventSelection` objects in order to produce histograms and measurements.

The `Analysis` loops over the individual events in each of the individual `AnalysisChains`, usually a data chain and several MC chains, and the complete `Analysis` object is written to a ROOT file. This file can then be reopened later to perform further analysis and subsequent studies.

6 A Study of $J/\psi \rightarrow \mu^+\mu^-$ Decays

The J/ψ analysis program uses a pre-selected data sample taken from 2005 which has been reprocessed by passing it through the current H1 calibration procedures, in order to analyse J/ψ decays in which a pair of muons are detected in the central tracking detector and in the forward tracking detector.

The program is structured such that the user initially decides whether they would like to analyse vertex fitted or non-vertex fitted muon tracks. Since by definition the extrapolations of non-vertex muon tracks are not required to pass through the vertex position, the accuracy with which we can determine the origin of these muons is somewhat limited.

The analysis program searches for tracks in the central tracking detector, disregarding any electron tracks and only accepting those muon tracks that have passed stringent quality control checks and have a transverse momentum greater than 0.8 GeV. If no suitable muon tracks are found in the central tracking detector, that particular run is stopped and the event is not analysed any further. However, if a suitable central muon track is found, the program continues with a search for the partnering muon track in the forward tracking detector. The programmming code required to perform this search is much the same as that for the central muon track, and thus there are another set of track selection criteria for the forward muon.

Crucially, this forward going muon can be detected within the iron return yoke and the forward tracking detector, each of which shares a common set of track selection criteria. Indeed it is the effect of these various track selections upon which the investigation is based.

As the J/ψ analysis program currently stands, some of these track selections cannot be applied to both vertex fitted muon tracks and non-vertex fitted muon tracks, and so depending upon whether the tracks are required to be vertex fitted or non-vertex fitted, a small amount of 'fine tuning' is necessary prior to running the analysis.

From the data events that pass through these numerous track selections, the efficiency of the forward tracking detector and the resolution of the J/ψ signature peak are determined. At the end of each analysis, a series of histograms are produced, the ones which are of particular importance to the investigation are listed below.

- The efficiency of the forward tracking detector[1].
- The individual efficiencies of the three supermodules which are situated within the forward tracking detector - these are the SM0, SM1 and SM2 with increasing z through the FTD.
- The invariant mass of the central muon and its partnering FTD muon.
- The invariant mass of the central muon and its partnering FTD muon, after including a 3% dead material correction to the momentum of the muon in the FTD.

In addition to these histograms, I added further histograms showing the transverse momenta of each muon (p_t), the polar angle of each muon (θ), the minimal radial starting position of the track (r_0), the chi squared of the track fit (χ^2) and the length of the track in the forward tracking detector (FTD*length*), for both the first (CTD) muon and second (FTD) muon prior to the application of any track selection conditions. The p_t and θ distributions are shown in figure 6. This 'raw' data not only indicates the range of values for each variable, but also allows us to make sure that each pair of muons is behaving exactly as expected before proceeding any further with the analysis.

It was known prior to the investigation that regardless of whether we pre-select vertex fitted muon tracks or non-vertex fitted tracks, that a high FTD efficiency and a suitably narrow J/ψ signature peak are mutually exclusive, and they cannot both be acheived simultaneously. Furthermore, as the detector efficiency improves the peak resolution consequently suffers and vice versa. The objective is therefore to investigate which track selections will provide the optimal balance bewteen an acceptable efficiency and an acceptable resolution.

[1] Although this could be considered a slightly unfair measurement of the FTD performace as the tracks in the iron yoke are non-vertex fitted, the tracks in the FTD are vertex fitted, and yet the efficiency has been calculated by the number of tracks in the FTD divided by the sum of the number of tracks in both the iron yoke and the FTD.

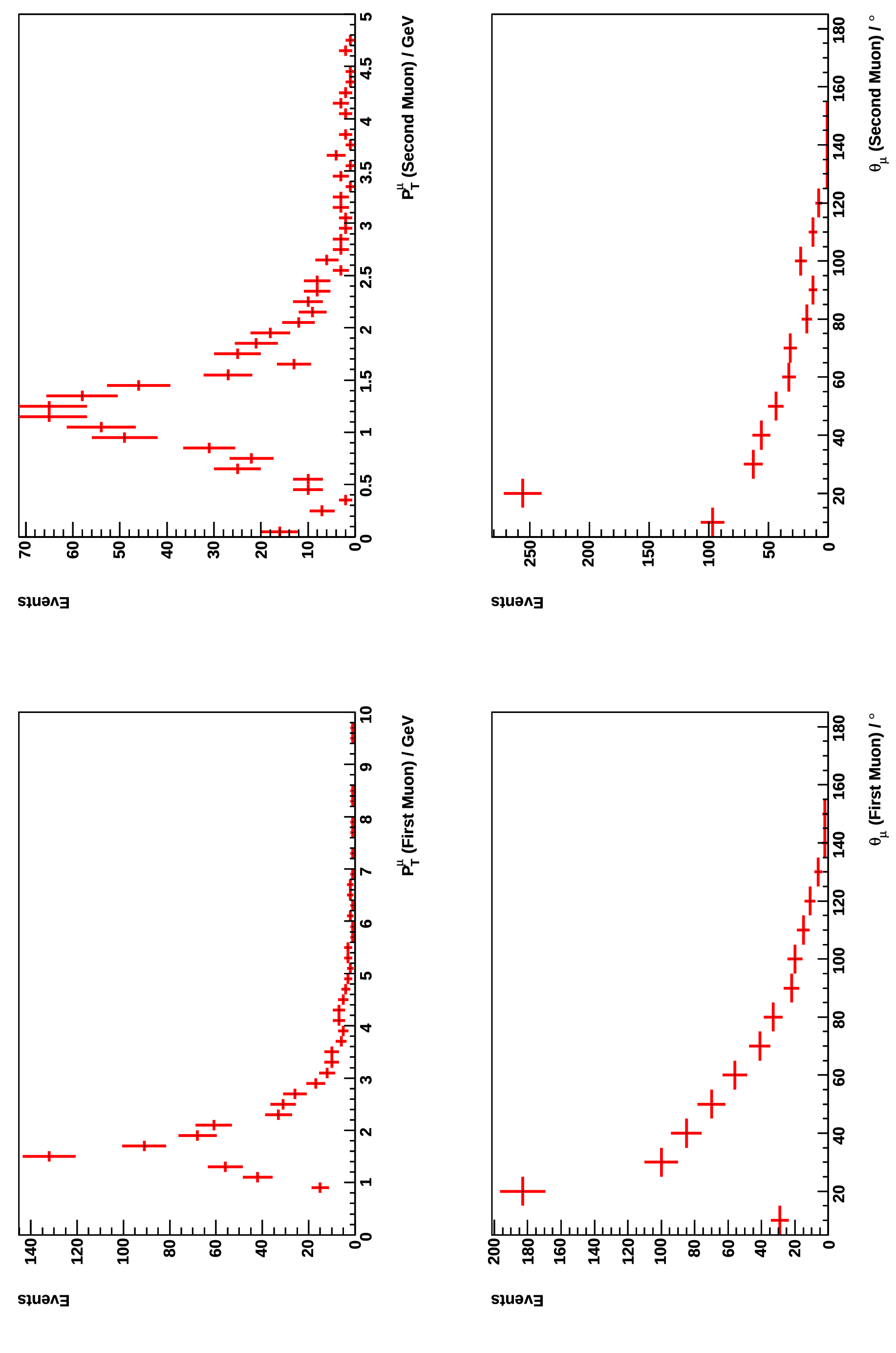

Figure 6: Histograms showing the values of the transverse momenta and the angles of the track trajectories for both the first (CTD) and second (FTD) muons prior to the implementation of any track selection cuts.

7 Results

Since each of the aforementioned variables are independent of one another their individual effects on the efficiency of the FTD and the resolution of the J/ψ signature peak can be determined by placing sensible cuts on each variable, (one at a time), and then observing the corresponding effects when the analyses are run. The values of these cuts can then be increased or decreased and again the subsequent effects on the detector efficiency and peak resolution can be observed.

These processes were indeed carried out for muons with both vertex fitted tracks and non-vertex fitted tracks, and the qualitative effects of placing various selection cuts on each of these variables are described below.

- **Transverse Momentum ($\mathbf{p}_t$)**

  For cuts allowing only high transverse momenta, the efficiency of the FTD is relatively low and the resolution of the J/ψ signature peak is reasonable. As the value of the minimum permitted transverse momentum is reduced, more events are observed, the detector efficiency improves and the resolution of the J/ψ peak decreases.

  Below a certain threshold (of the order of 0.001 GeV), the efficiency of the FTD and the peak resolution remain unaffected. This is observed to be the case for both the vertex fitted muon tracks and the non-vertex fitted muon tracks, although it was interesting to note that when only tracks with high transverse momenta are selected, secondary peaks begin to appear at approximately 3.9 GeV for vertex fitted tracks and 4.5 GeV for non-vertex fitted tracks.

  Similarly, deeper investigations showed that the 0.001 GeV transverse momentum threshold is not observed for one of the FTD's supermodules when analysing non-vertex fitted tracks. This is the SM1 supermodule, the efficiency of which continues to increase as the value of the minimum permitted transverse momentum is lowered below the threshold.

- **Polar Angle of Track Trajectory (θ)**

  When the range of permitted track trajectory angles is made narrower the number of entries falls, the efficiency of the FTD decreases and the peak resolution improves. Introducing cuts which allow broader and broader angle ranges have almost no effect on the detector efficiency, due to the acceptance of the FTD, although the resolution of the J/ψ peak is seen to slightly increase. This is observed to be the case for both the vertex fitted muon tracks and the non-vertex fitted muon tracks.

  Interestingly, the small shoulder that had previously appeared next to the J/ψ resonance (at approximately 5 GeV), disappears when the permitted angle of trajectory is increased to particularly high ranges.

- **Radius of the Track Starting Position ($\mathbf{r}_0$)**

  For restrictions allowing only low r_0 values, the efficiency of the FTD is relatively poor, the resolution of the J/ψ is good and a small secondary peak is observed in the invariant mass plot at approximately 2.2 GeV. Conversely, as the cut is altered to permit higher r_0 values, more events are observed, the FTD efficiency improves, the resolution of the peak becomes increasingly worse and again a very small shoulder is observed in the invariant mass plot at approximatley 4.5 GeV. Note that this cut could only be applied to the vertex fitted tracks and not the non-vertex fitted tracks.

- **Chi Squared (χ^2)**

  For cuts permitting only low χ^2 values, that is demanding a higher quality fit track, fewer events are observed and the efficiency of the FTD is poor, but the resolution of the J/ψ peak is more than sufficient. As the cut is altered to permit higher chi squared values, the FTD efficiency improves and the resolution of the peak decreases, until a threshold cut value is reached above which point the efficiency and the resolution remain unchanged.

  This behaviour is observed for both the vertex fitted muon tracks and the non-vertex fitted muon tracks, although it is interesting to note that in the case of non-vertex fitted tracks, the efficiency of one of the FTD's supermodules, the SM0 supermodule, remains almost constant througout. Also, as has been the case with some of the previously investigated variables, restrictions allowing only particulalrly low values results in the appearance of a secondary peak in the invariant mass plot. This peak can be found close to the J/ψ resonance at an invariant mass value of approximately 5 GeV.

- **Track Length in the Forward Tracking Detector (FTD*length*)**

  For cuts allowing a broad range of track lengths, the efficiency of the FTD is relatively high and the resolution of the J/ψ peak is slightly poor. Then, as the value of the minimum permitted track length is increased, fewer events are observed, the FTD efficiency falls and the resolution of the peak improves slightly. Note that this cut can only be applied to the vertex fitted tracks and not the non-vertex fitted tracks.

From observing the effects on the FTD efficiency and the J/ψ resolution of changing the values of the cuts on these variables, it was possible to determine a set of optimum selection cuts that provide a good balance between efficiency and resolution (see chapter 8).

It is also worth mentioning that although the vertex fitted muon tracks and non-vertex fitted muon tracks behave as described above, there were some noticable differences between the plots generated from each of these muon track types. In particular, when using non-vertex fitted muon tracks the efficiency of the FTD was generally greater than that when using vertex fitted tracks. Similarly, the resolution was generally a lot better when using vertex fitted muon tracks in comparison to studies of non-vertex fitted muon tracks. The number of events was also observed to be higher in those plots generated using the non-vertex fitted muon tracks.

All these features are a consequence of the fundamental difference between vertex fitted and non-vertex fitted muon tracks. For example if we concentrate on non-vertex fitted tracks, the process of selecting suitable muon tracks is much looser and there is a larger margin for error in comparison to when we study vertex fitted muon tracks. Subsequently, tracks enter the analysis process that should have ideally been filtered out, and thus the number of events observed is obviously higher than when we use vertex fitted muon tracks. Similarly, since we cannot guarantee that all these analysed tracks are originating from J/ψ decays, the width of the resonance in the invariant mass plot is therefore a lot wider than when we analyse vertex fitted tracks. Also, since the number of events passed into the analysis is higher when using the non-vertex fitted tracks the calculated efficiency of the FTD is subsequently higher than if we had studied vertex fitted tracks.

Figure 7 shows three plots of the FTD efficiency as a function of its angular range: figure 7a shows the efficiency for vertex fitted muon tracks with the additional track selections; figure 7b shows the efficiency for vertex fitted muon tracks without additional track selections and finally figure 7c shows the efficiency for non-vertex fitted muon tracks without additional track selections. Figure 8 shows three plots (for similar track requirements as described above) of the invariant masses of the muon pairs, after applying corrections for dead material present within the detector.

As is expected, the greater the number of track selections the fewer events are observed and thus the smaller the detector efficiency. Even with no additional track selection criteria the requirement of vertex fitted muon tracks is a selection within itself, and thus the highest FTD efficiencies are achieved through analyses of non-vertex fitted tracks. However as the track selections become looser, more tracks are misidentified as muons and hence the J/ψ resonance becomes wider. Subsequently, the highest resolutions are obtained when all the muon track selection cuts are applied.

The decision as to whether one uses vertex fitted or non-vertex fitted muon tracks is therefore dependent upon the problem at hand. If the investigation requires a high detector efficiency, then the analyses can be carried out using non-vertex fitted tracks. Similarly, if the investigation requires an accurate J/ψ peak, then the vertex fitted tracks muon tracks can analysed instead. Also note that as well as initially choosing which track types to analyse, the default track selections (determined here in this report) can also be adjusted accordingly, to fine tune the track selection processes prior to the main analysis being performed.

In general, the resolution of the J/ψ peak originating from a non-vertex fitted track analysis is much worse that that from a vertex fitted track analysis. And although the efficiency of the detector is greater using non-vertex fitted tracks, this still cannot justify their inclusion in the default track selection. Subsequently, the vertex fitted muon tracks were chosen to appear in the default track selection for the H1TrackFinder (see chapter 8).

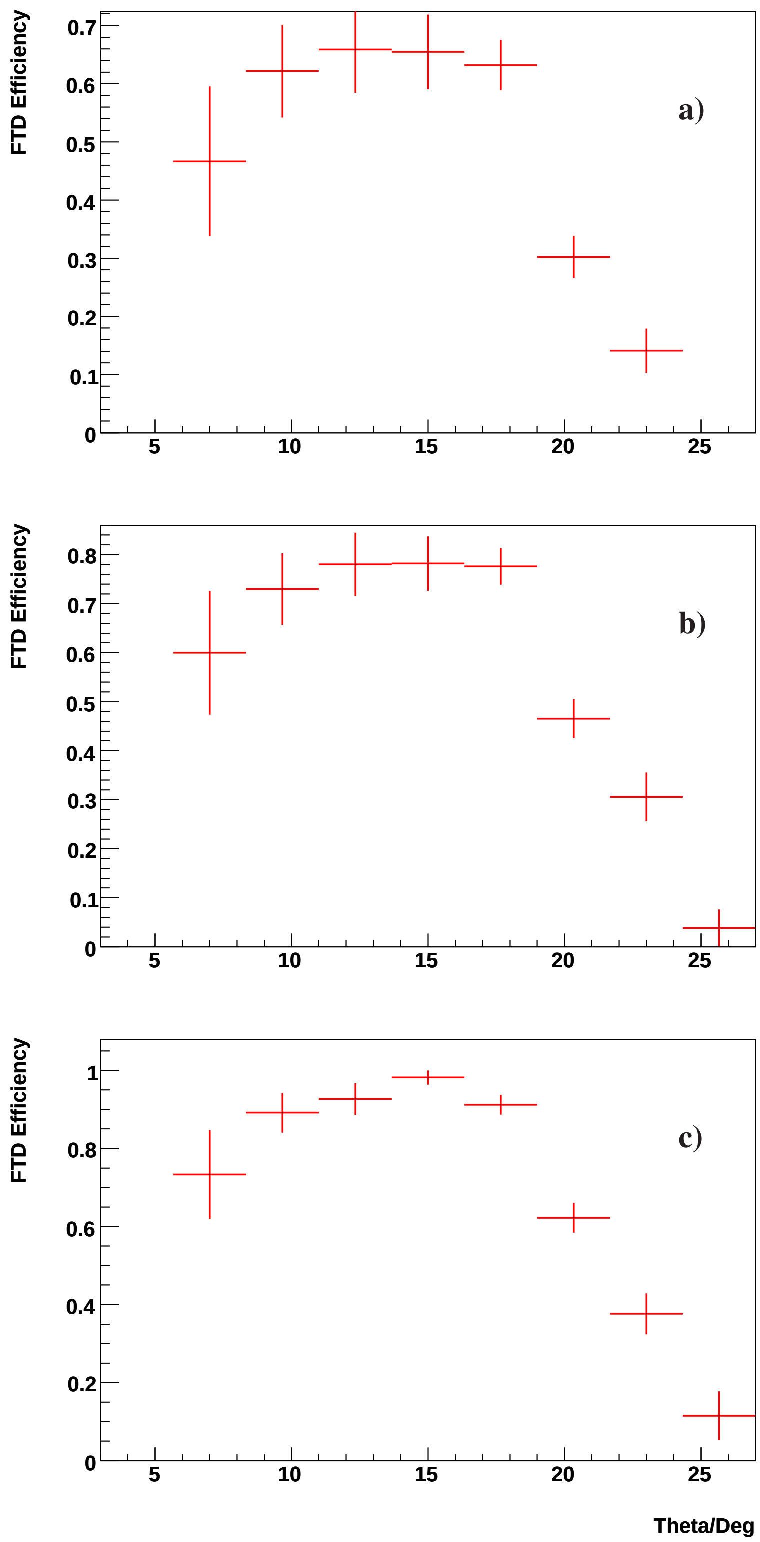

Figure 7: The FTD track reconstruction efficiency for a) vertex fitted muon tracks with additional selection criteria; b) vertex fitted muon tracks with no additional track selection criteria; c) non-vertex fitted muon tracks with no additional track selection criteria.

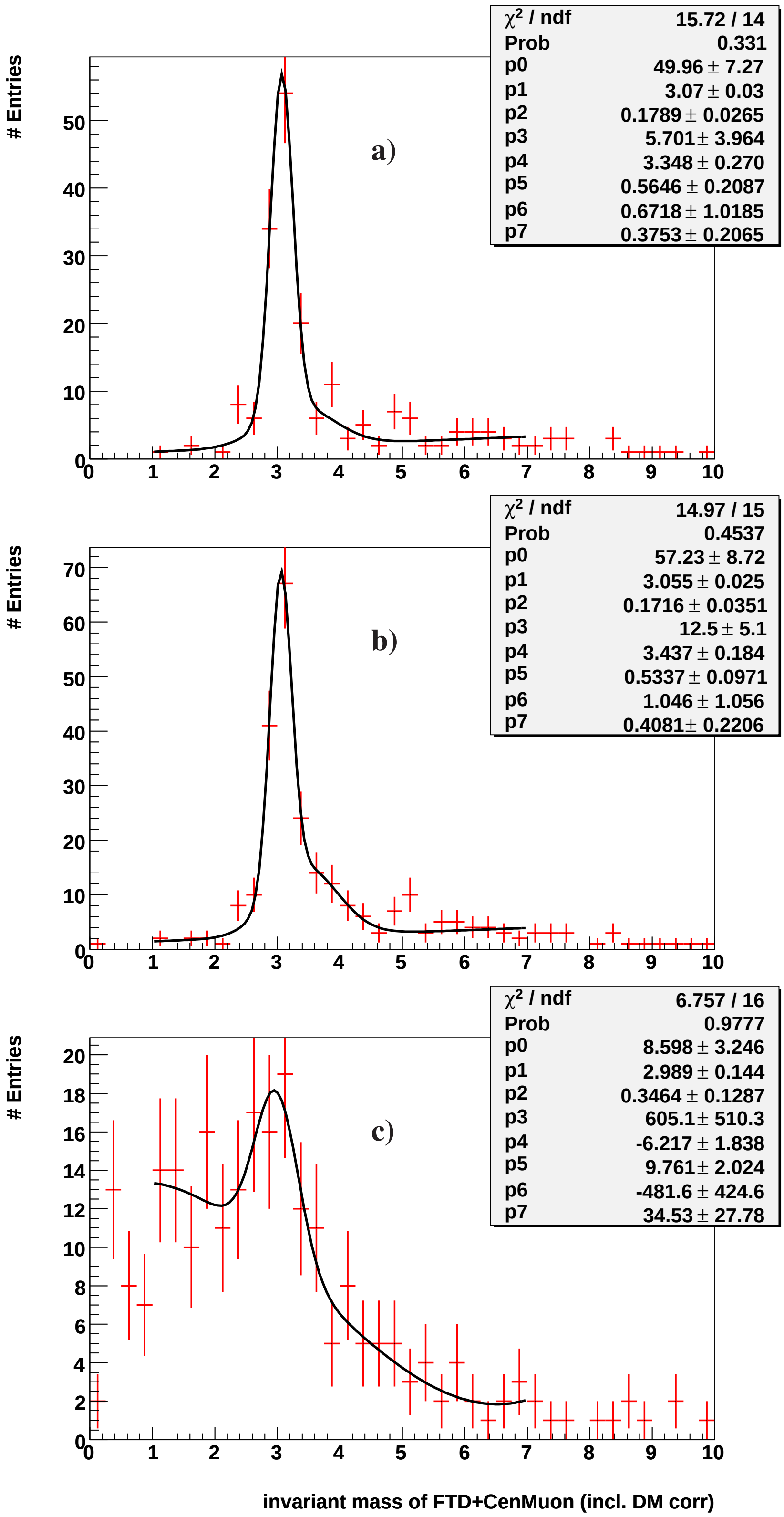

Figure 8: The reconstructed J/ψ peak for a) vertex fitted muon tracks with additional selection criteria; b) vertex fitted muon tracks with no additional track selection criteria; c) non-vertex fitted muon tracks with no additional track selection criteria. P0, P1 and P2 indicate the number of J/ψ candidates, the mean of the value of the J/ψ peak (in GeV) and the width of the J/ψ peak (in GeV).

8 Conclusion

The default track selections to be placed on the vertex fitted muon tracks are:

$$\mathrm{p}_t > 0.001 \text{ GeV}$$
$$6\,^\circ \leq \theta \leq 25\,^\circ$$
$$\chi^2 < 25$$
$$\mathrm{r}_0 < 10 \text{ cm}$$
$$(\frac{dp}{p}) \leq 9999.9 \text{ GeV \&\& p} \geq 0.5 \text{ GeV}$$

In discussing the results with my supervisor, it was decided that the cut on the FTD*length* would be disregarded with respect to the default track selection. Furthermore, it also became apparent that an additional cut would be required that had not been studied in this investigation, which is listed last in the above selection, whereby each muon track momentum measurement must be greater than 500 MeV, and that the error on this value is sensible.

In conclusion this project has been both thoroughly enjoyable and highly productive. My initial involvement in the C++ programming tutorials were particularly helpful as there were many aspects of the project with which I was not familiar prior to my arrival at DESY. Considering that I initially knew nothing of Linux, ROOT, the C++ programming language and the H1OO Analysis Framework I will complete the summer student program having learnt plenty about what a career in particle physics actually involves.

In the first few weeks, one of the primary tasks set by my supervisor was to investigate the analyses performed in basic packages such as the *H1AnalysisExample* package; whilst he simultaneously introduced me to the various classes of the *H1OO framework* and how they are interlinked. By altering the J/ψ analysis program so that it could plot the histograms of a few additional variables, (in much the same way as was done in this investigation), I gradually came to understand how the programming code for such analyses was structured.

When my supervisor presented me with the details of my main project at DESY, it was easy to see the connections between the J/ψ *analysis* package and the *H1AnalysisExample* package that I first encountered. Unlike the previous packages the J/ψ analyses were not applied to MC data or generator level data and as a result only one analysis data chain, for the reconstucted data, was analysed. Each analysis was subsequently completed in a few seconds, allowing me to study the effects of different selection cuts and learn more about the physics of these J/ψ decay processes.

Of course if more time was available then I could have studied a wider range of cuts and thus found a more suitable optimum track seletion; although I think that the investigation was performed thoroughly enough to be of some use to those physicists who are involved in the performace of the FTD.

All in all, I have had a wonderful time at DESY and I have learnt an awful lot more than I expected to in just two months; not only concerning the various branches of particle physics that I have been introduced to, but also the general working environment of a particle physicist. The latter of which has proved to be of great significance as I have since decided to pursue a career in particle physics.

9 Acknowledgements

Firstly, I would like to thank my supervisor David South for not only teaching me about this particular project topic but also for giving me a valuable insight into the life of a particle physicist. I would also like to thank Matthew Beckingham for often providing me with much needed advice. Thanks to Hannes Jung for always offering his help in the countless times I ran into programming cul-de-sacs, and I must also express my gratitude to Joachim Meyer who provided me with the oppertunity to become a DESY summer student in the first place.

Special thanks goes to all the summer students (partcularly Plamen Hopchev) who along with David and Matthew, made my stay in Hamburg a most enjoyable one.

References

[1] LHC General Infomation, *http://lhc.web.cern.ch/lhc/generation/gen_info.htm*

[2] The H1 Collaboration, *The H1 Detector at HERA*, NIM, **A386** (1997) 310 and 348.

[3] https://www-h1.desy.de/icas/oop/

[4] The ROOT Homepage at CERN *http://root.cern.ch*
The ROOT Homepage at FERMILAB *http://www-pat.fnal.gov/root/*

[5] Paul Laycock, David South, *A Generic Analysis Framework for H1*, (2005).

[6] *http://www-h1.desy.de/icas/oop/roothtml/current/ClassIndex.html*